Optical spectra from a degenerate optical parametric oscillator coupling with N two-level atoms

Shaozheng Jin and Min Xiao

Department of Physics, University of Arkansas, Fayetteville, Arkansas 72701

We study transmitted optical spectra from a realistic system which consists of a degenerate optical parametric oscillator (DOPO) and N two-level atoms. Optical bistability appears when parameters are suitable. Below the modified threshold of the DOPO (lower turning point of the bistable curve), the coherent intensity is always zero at the lower branch, which allows us to describe this system with a set of linear differential equations. By transforming the field and atomic variables into corresponding quadratures, we find that, for the resonance case, one atomic quadrature will only couple to one field quadrature. By separating these two quadratures, we are able to study the effects due to squeezed and unsqueezed quadratures on the atoms. The optical and atomic spectra of this system are obtained, analytically, for arbitrary coupling strength and cavity linewidth.

I. INTRODUCTION

Subnatural atomic linewidth has been predicted in several systems [1–4]. For different systems, the atomic linewidth narrowing comes from different mechanisms. When a single two-level atom is placed in a squeezed vacuum, the atomic polarization decay rate will be split into two distinguishable rates, with one going to zero and other to infinity as the degree of squeezing increases [1]. This original prediction by Gardiner has created a great deal of interest in this subject and numerous theoretical papers were published since then [2]. Rice and Carmichael have shown that a subnatural linewidth also occurs in ordinary resonance fluorescence, in the absence of the squeezed vacuum [4]. In this case, squeezed light does not irradiate the atom. Squeezed light is produced in the interaction between the driven atom and the modes of the usual vacuum. When one or many two-level atoms are placed in an optical cavity and driven by an external field (atomic optical bistability or AOB), the atomic linewidth narrowing can come from two different sources, as discussed by Carmichael et al. [3]. When the cavity field and the atoms are strongly coupled, the composite system will decay with an averaged decay rate of the cavity and the atoms. If the cavity field decays much more slowly than the atoms, the transmitted or fluorescence spectra will be dominated by the atomic decay, which will approach one-half of the natural atomic decay rate. Other than this dynamic averaging effect, squeezing produced in this interaction will also contribute to a maximum of 36% linewidth narrowing to the optical spectra. The atomic linewidth narrowing in this system was experimentally observed in the transmitted optical spectrum [5].

In this paper, we consider a different system, which consists of a degenerate optical parametric oscillator (DOPO) and N two-level atoms [6]. Since DOPO is a "perfect squeezer" [7], we study how this squeezed cavity mode affects the atomic spectra and how the atoms affect the squeezed spectra for different coupling strengths and arbitrary cavity linewidths. At a weak interaction limit, atoms will not change the squeezed cavity field much when the external pumping power is just below the modified DOPO threshold value. The situation is similar to atoms inside a partially squeezed vacuum or atoms driven by a squeezed field. In the strong-coupling limit, the field and the atoms will affect each other and we have to consider this system as a composite one. In such a case, the dynamic averaging effect will play an important role. The essential difference between this system and the one studied by Carmichael et al. (atoms inside an optical cavity driven by an external field) [3] is the phase-sensitive gain feature near and above the DOPO threshold. It is this phase-sensitive gain that produces the optimal squeezing near the DOPO threshold. In some respects, this system resembles the model of a laser with a saturable absorber, but with a phase-sensitive gain.

Agarwal and Gupta studied a similar system. They considered the cavity field as a reservoir and atoms as an effective harmonic oscillator [8]. Using a Wigner function, they calculated the optical spectra from such a system. Several assumptions and shortcomings were present in that paper. First, due to the initial assumption of the atoms being a harmonic oscillator, their method cannot be used to analyze the steady-state dynamic behavior of the field modes; for example, they cannot predict the bistability of the output intensity versus the pumping intensity. Second, they did not consider the modification of the DOPO threshold due to the atomic absorption. Third, they only considered the resonance case with no atomic detuning. Fourth, in their calculation, they always took the adiabatic limit in which the atomic linewidth is zero. Finally, in that calculation, the effects of squeezed and unsqueezed quadratures on the atoms were not clear.

We start with a general Hamiltonian to derive a set of nonlinear differential equations [6]. Steady-state solutions of this system exhibit bistability in the output intensity versus pumping intensity. We calculate the new threshold of the DOPO modified by the atomic absorp-

tion. The intracavity steady-state intensity below the lower turning point of the bistability curve (same as the modified DOPO threshold) is always zero, although the intensity fluctuations can be quite large, which is different from the AOB. We discuss the most interesting region, which stays between the unmodified DOPO threshold and the modified DOPO threshold (lower turning point of the bistable curve).

By using Schwinger representation [9] at the lower branch of the bistable curve where the steady-state intensity is always zero, we are able to write down a set of coupled linear operator equations for the field operators and atomic polarization operators. By transforming both field and atomic operators into selected quadratures, we find that, at resonance, these operator equations separate into two independent pairs of equations. The squeezed field quadrature of the DOPO couples only to one atomic quadrature, and the unsqueezed quadrature of the DOPO couples to the other atomic quadrature. This separation gives a clear picture of how the squeezed and unsqueezed field quadratures of the DOPO affect the atomic dynamics. We have obtained simple analytic expressions of optical spectra for arbitrary cavity linewidth and coupling strength between the atoms and the field.

The arrangement of this paper is as follows. In Sec. II, we introduce the Hamiltonian and give the steady-state solutions. In Sec. III, we derive a set of dynamic operator equations using Schwinger representation in the lower branch of the bistable curve. In Sec. IV, we calculate both atomic and field transmission spectra and the field intensity from each of the field quadratures. Section V serves as a conclusion.

II. MODEL AND STEADY-STATE SOLUTIONS

We consider a DOPO system consisting of a pair of nonlinear crystals placed inside an optical cavity. Two crystals ($KNbO_3$, for example) are needed to compensate the walk-off effect for different frequencies. An atomic beam goes through the middle of these two crystals. The cavity is pumped by a strong external coherent field at near twice the atomic transition frequency.

The Hamiltonian of this composite system, under the electric-dipole and rotating-wave approximations, can be written as [6]

$$\hat{H} = \sum_{i=1}^{7} \hat{H}_i \ ,$$

$$\hat{H}_1 = \hbar\omega_c \hat{a}^{\dagger}\hat{a} + \tfrac{1}{2}\hbar\omega_a \sum_{\mu} \hat{\sigma}_{\mu}^{z} + \hbar\omega_2 \hat{a}_{2}^{\dagger}\hat{a}_2 \ ,$$

$$\hat{H}_2 = i\hbar \sum_{\mu} g(\hat{a}^{\dagger}\hat{\sigma}_{\mu}^{-}e^{-i\phi} - \hat{a}\,\hat{\sigma}_{\mu}^{+}e^{i\phi}) \ ,$$

$$\hat{H}_3 = i\hbar\frac{\kappa}{2}(\hat{a}^{\dagger 2}\hat{a}_2 - \hat{a}^{2}\hat{a}_{2}^{\dagger}) \ ,$$

$$\hat{H}_4 = \sum_{\mu} (\hat{\Gamma}_{a}^{-}\hat{\sigma}_{\mu}^{+} + \hat{\Gamma}_{a}^{+}\hat{\sigma}_{\mu}^{-} + \hat{\Gamma}_{p}\hat{\sigma}_{\mu}^{z}) \ ,$$

$$\hat{H}_5 = \hat{a}_2\hat{B}_{2}^{\dagger} + \hat{a}_{2}^{\dagger}\hat{B}_2 \ ,$$

$$\hat{H}_6 = \hat{a}\,\hat{B}_{1}^{\dagger} + \hat{a}^{\dagger}\hat{B}_1 \ ,$$

$$\hat{H}_7 = i\hbar(\epsilon_2\hat{a}_{2}^{\dagger}e^{-i\omega_p t} - \epsilon_{2}^{*}\hat{a}_2 e^{i\omega_p t}) \ ,$$

(1)

where $\hat{H}_1$ is the free energy of the fields and atoms, $\hat{H}_2$ is the interaction between the atoms and the subharmonic field, $\hat{H}_3$ describes the DOPO process, $\hat{H}_4$ is the atomic decay, $\hat{H}_5$ is the decay of the field at the pumping frequency, $\hat{H}_6$ is the decay of the subharmonic field, and $\hat{H}_7$ is the pumping term. $\hat{a}_{2}^{\dagger}$ and $\hat{a}_2$ denote the creation and annihilation operators, respectively, of the fundamental field mode. $\hat{a}^{\dagger}$ and $\hat{a}$ denote the creation and annihilation operators, respectively, of the subharmonic frequency. $\hat{\sigma}^{\pm}$, $\hat{\sigma}^{z}$ are the atomic operators, ω_a is the atomic transition frequency and ω_c the frequency of the cavity subharmonic field. g is the coupling constant between atoms and the intracavity field. κ is the coupling coefficient of the nonlinear process of the crystals. $\hat{\Gamma}_{a}^{\pm}$ and $\hat{\Gamma}_p$ are the noise operators of the atoms. $\hat{B}_{2}^{\dagger}$ and $\hat{B}_2$ are the noise operators of the fundamental field mode, and $\hat{B}_{1}^{\dagger}$ and $\hat{B}_1$ are the noise operators of the subharmonic field mode. ϵ_2 is the complex classical amplitude of the external driving field.

To derive a Fokker-Planck equation from this Hamiltonian is a standard technique [10]. In that procedure, we translate all the operators into the corresponding c numbers defined by

$$(\hat{a},\hat{a}^{\dagger},\hat{a}_2,\hat{a}_{2}^{\dagger},\hat{J}^{-},\hat{J}^{+},\hat{J}^{z}) \rightarrow (\alpha,\alpha^{\dagger},\alpha_2,\alpha_{2}^{\dagger},J^{-},J^{+},J^{z}) \equiv \mathbf{u} \ ,$$

where

$$\hat{J}^{z} \equiv \sum_{\mu} \hat{\sigma}_{\mu}^{z} \quad \text{and} \quad \hat{J}^{\pm} \equiv \sum_{\mu} e^{\pm i\mathbf{\kappa\cdot r}}\hat{\sigma}_{\mu}^{\pm} \ . \tag{2}$$

From that Fokker-Planck equation, we can get a set of equations of motion for the variables in the following forms [6]:

$$\frac{d\alpha}{dt} = -(\gamma_1 + i\Delta_c)\alpha + gJ^{-} + \kappa\alpha^{\dagger}\alpha_2 + \Gamma_{\alpha}(t) \ ,$$

$$\frac{d\alpha^{\dagger}}{dt} = -(\gamma_1 - i\Delta_c)\alpha^{\dagger} + gJ^{+} + \kappa\alpha\alpha_{2}^{\dagger} + \Gamma_{\alpha^{\dagger}}(t) \ ,$$

$$\frac{d\alpha_2}{dt} = -(\gamma_2 + i\Delta_2)\alpha_2 - \frac{\kappa}{2}\alpha^2 + \epsilon_2 \ ,$$

$$\frac{d\alpha_{2}^{\dagger}}{dt} = -(\gamma_2 - i\Delta_2)\alpha_{2}^{\dagger} - \frac{\kappa}{2}\alpha^{\dagger 2} + \epsilon_{2}^{*} \ , \tag{3}$$

$$\frac{dJ^{-}}{dt} = -\left[\gamma_p + \frac{\gamma_{\parallel}}{2} + i\Delta_a\right]J^{-} + g\alpha J^{z} + \Gamma_{-}(t) \ ,$$

$$\frac{dJ^{+}}{dt} = -\left[\gamma_p + \frac{\gamma_{\parallel}}{2} - i\Delta_a\right]J^{+} + g\alpha^{\dagger}J^{z} + \Gamma_{+}(t) \ ,$$

$$\frac{dJ^{z}}{dt} = -\gamma_{\parallel}(J^{z} + N) - 2g(J^{-}\alpha^{\dagger} + J^{+}\alpha) + \Gamma_{z}(t) \ ,$$

where

$$\langle \Gamma_{\alpha}(t)\Gamma_{\alpha}(t') \rangle = \kappa\alpha_2\delta(t - t') \ ,$$

$$\langle \Gamma_{\alpha^{\dagger}}(t)\Gamma_{\alpha^{\dagger}}(t') \rangle = \kappa\alpha_{2}^{\dagger}\delta(t - t') \ , \tag{4}$$

$$\langle \Gamma_{\alpha}(t)\Gamma_{\alpha^{\dagger}}(t') \rangle = \langle \Gamma_{\alpha^{\dagger}}(t)\Gamma_{\alpha}(t') \rangle = 0 \ ,$$

and

$$\langle \Gamma_-(t)\Gamma_-(t')\rangle = 2g\alpha J^-\delta(t-t') \ ,$$

$$\langle \Gamma_+(t)\Gamma_+(t')\rangle = 2g\alpha^\dagger J^+\delta(t-t') \ , \qquad (5)$$

$$\langle \Gamma_z(t)\Gamma_z(t')\rangle = [2\gamma_\parallel(J^z+N)$$
$$-4g(J^+\alpha+J^-\alpha^\dagger)]\delta(t-t') \ ,$$

where $\Delta_c=\omega_p/2-\omega_c$, $\Delta_2=\omega_p-\omega_2$, and $\Delta_a=\omega_p/2-\omega_a$. For simplicity, we consider a double resonant cavity such that $\Delta_c=0$, $\Delta_2=0$, and $\Delta_a=\omega_c-\omega_a$. We will also neglect the collisional decay rate γ_p and write $\gamma_p+\gamma_\parallel/2=\gamma_\perp$. $\gamma_\perp$ is the atomic polarization decay rate. γ_1 is the cavity decay rate of the subharmonic field and γ_2 the cavity decay rate of the fundamental field mode. N is the total number of atoms in the cavity mode.

The steady-state solutions of Eqs. (3) can be found to be

$$\left[1+\frac{2C}{1+\Delta^2+X}+rX \right]^2 + \left[\frac{2C\Delta}{1+\Delta^2+X} \right]^2 = Y$$

and

$$X=0 \ , \qquad (6)$$

where several normalized parameters are introduced and defined as follows:

$$\Delta \equiv \frac{\Delta_a}{\gamma_\perp}, \quad C \equiv \frac{Ng^2}{2\gamma_\perp\gamma_1}, \quad N_s \equiv \frac{\gamma_\perp\gamma_\parallel}{4g^2} \ ,$$
$$n_0 \equiv \frac{2\gamma_1\gamma_2}{\kappa^2}, \quad |\epsilon_0| \equiv \frac{\gamma_1\gamma_2}{\kappa} \ . \qquad (7)$$

The normalized field variables are

$$x \equiv \frac{\alpha}{\sqrt{N_s}}, \quad X \equiv xx^*, \quad y \equiv \frac{\epsilon_2}{\epsilon_0}, \quad Y \equiv yy^* = \left| \frac{\epsilon_2}{\epsilon_0} \right|^2 . \qquad (8)$$

$r \equiv N_s/n_0$ is a measure of the relative strength of the atomic system over the DOPO. It is obvious that, as $\Delta \to \infty$ or $\Delta \gg X$ and C, Eq. (6) goes back to the normal DOPO form. One of the most obvious differences between the steady-state Eqs. (6) and the steady-state equation of the atomic optical bistability (AOB) system is that $X=0$ is one steady-state solution for any pumping power due to the DOPO process [11].

The threshold value of the pumping amplitude for subharmonic generation in this coupling system will be modified by the atoms as

$$|\bar{\epsilon}^c| = |\epsilon_0| \left[\left[\frac{2C\Delta}{1+\Delta^2} \right]^2 + \left[1+\frac{2C}{1+\Delta^2} \right]^2 \right]^{1/2} . \qquad (9)$$

Due to atomic absorption, the DOPO threshold is increased. In the resonance interaction case ($\Delta=0$), we will obtain the maximum threshold value of

$$|\bar{\epsilon}^c_{max}| = |\epsilon_0|(1+2C) \ . \qquad (10)$$

The additional term of $2C$ for the resonance case is due to energy loss through the atomic fluorescence.

A particular bistable curve related to the steady-state Eqs. (6) with $\Delta=1.4$, $C=10$, and $r=0.2$ is given in Fig. 1.
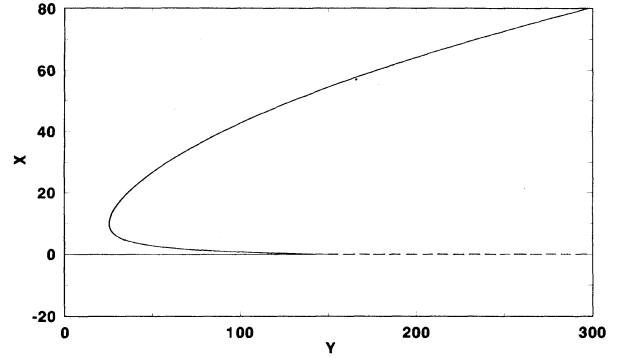
FIG. 1. Typical bistable curve of intracavity intensity X vs pumping intensity Y, with $\Delta=1.4$, $C=10$, and $r=0.2$. On the lower branch, the intracavity intensity is always zero ($X=0$).

There are multivalues of X for a given pumping intensity Y in the region just below the modified DOPO threshold value. The stability analysis for these steady-state solutions shows that this system is a standard bistable device in the so-called good-cavity limit ($\gamma_1 \ll \gamma_\perp$) [6]. When this system satisfies

$$\mu C > \tfrac{1}{2} \ , \qquad (11a)$$

where $\mu=\gamma_1/\gamma_\perp$ is the parameter describing cavity quality relative to the atomic polarization decay rate, the steady-state intracavity field will not be stable all the way up to the modified threshold value $1+2C$. The system will become unstable at

$$y = \frac{1+\mu}{\mu} < 1+2C \ . \qquad (11b)$$

Under conditions (11a) and (11b), the system will experience Hopf bifurcation, which will not be discussed here. The reason for this instability can be understood in the following way. When the atomic decay rate is large, the subharmonic field photons produced in the parametric down-conversion process will be brought out by atomic fluorescence. In such a case, the intracavity subharmonic field will not build up until the atoms are saturated at the turning point, where the intracavity field starts to oscillate. If the atomic decay rate is not much larger than the cavity decay rate, then the atoms cannot dump all the photons produced by the down-conversion process fast enough, which causes the cavity field to oscillate before the lower turning point. In such a case, the intracavity intensity will jump from the lower branch to the upper branch before the atoms are saturated. The dynamics of this instability will be left to a future paper.

III. DYNAMIC EQUATIONS AT THE LOWER BRANCH

When atoms are absent, the DOPO produces 50% intracavity squeezing near its threshold, which gives perfect squeezing at the output for a single-sided cavity. When atoms get into the cavity, the intracavity subharmonic field and the atoms will interact and form a composite system. In the weak-interaction limit, the atoms will not modify the intracavity field. This situation

resembles atoms inside a partially squeezed reservoir. However, under the strong-interaction limit, the cavity field and the atoms will couple to each other and we can no longer consider them separately. The transmitted atomic and field spectra will be greatly altered. We will discuss these limits and the resulting spectra for different parameter regions.

In the following, we will concentrate mainly on the most interesting region, e.g., on the lower branch near the lower turning point of the bistable curve. It is obvious that when atoms do not exist or the frequency detuning is very large, the lower turning point is the normal DOPO threshold, where squeezing has its maximum (50% for the intracavity field). It should be noted that a very important feature of this system is that, as far as the pumping field is below the modified threshold of this composite system as defined by Eq. (9), the steady-state intensity remains zero at the lower branch. This is very different from the AOB system [10], where the field intensity increases, as the driving field increases, to the value of $\sqrt{2CX}$ at the lower turning point. Of course, at exactly the threshold point or the instability point as discussed at the end of Sec. II, the pumping depletion will be very important and has to be taken into account.

At the lower branch of the bistable curve (but not exactly on the lower turning point), we can neglect pumping depletion and use the Schwinger representation for the atomic variables. In the weak-field limit, the atoms are mainly in their ground state, so we can approximate the collective atomic operators as [9]

$$\hat{J}_+ = \sqrt{N}\hat{b}^\dagger, \quad \hat{J}_- = \sqrt{N}\hat{b}$$

and   (12)

$$\hat{J}_z = (\hat{b}^\dagger \hat{b} - \tfrac{1}{2}N) ,$$

with the commutation relation

$$[\hat{b}, \hat{b}^\dagger] = 1 .$$ (13)

N is the number of atoms in the cavity mode.

Substituting these operators into the Hamiltonian (1), we can derive a set of operator equations that, after adiabatic elimination of $\hat{a}_2^\dagger$ and $\hat{a}_2$ (no depletion of the pumping field), take the forms

$$\frac{d\hat{a}}{dt} = -\gamma_1 \hat{a} + \sqrt{N}g\hat{b} + \frac{\kappa}{\gamma_2}\hat{a}^\dagger \epsilon_2 + \hat{\Gamma}_a(t) ,$$

$$\frac{d\hat{a}^\dagger}{dt} = -\gamma_1 \hat{a}^\dagger + \sqrt{N}g\hat{b}^\dagger + \frac{\kappa}{\gamma_2}\hat{a}\epsilon_2^* + \hat{\Gamma}_{a^\dagger}(t) ,$$

$$\frac{d\hat{b}}{dt} = -(\gamma_\perp + i\Delta_a)\hat{b} - \sqrt{N}g\hat{a} + \hat{\Gamma}_-(t) ,$$ (14)

$$\frac{d\hat{b}^\dagger}{dt} = -(\gamma_\perp - i\Delta_a)\hat{b}^\dagger - \sqrt{N}g\hat{a}^\dagger + \hat{\Gamma}_+(t) ,$$

with

$$\langle \hat{\Gamma}_a(t)\hat{\Gamma}_a(t')\rangle = \frac{\kappa}{\gamma_2}\epsilon_2\delta(t-t') ,$$

$$\langle \hat{\Gamma}_a^\dagger(t)\hat{\Gamma}_a^\dagger(t')\rangle = \frac{\kappa}{\gamma_2}\epsilon_2^*\delta(t-t') ,$$

$$\langle \hat{\Gamma}_a(t)\hat{\Gamma}_a^\dagger(t')\rangle = \langle \hat{\Gamma}_a^\dagger(t)\hat{\Gamma}_a(t')\rangle = 0 ,$$

$$\langle \hat{\Gamma}_+(t)\hat{\Gamma}_+(t')\rangle = \frac{2ga^\dagger b^\dagger}{\sqrt{N}}\delta(t-t') ,$$ (15)

$$\langle \hat{\Gamma}_-(t)\hat{\Gamma}_-(t')\rangle = \frac{2gab}{\sqrt{N}}\delta(t-t') ,$$

$$\langle \hat{\Gamma}_+(t)\hat{\Gamma}_-(t')\rangle = \langle \hat{\Gamma}_-(t)\hat{\Gamma}_+(t')\rangle = 0 .$$

To simplify calculations and to study the dominant effects in this system, we will neglect the atomic fluctuations based on the following reasons. One reason is that, at the lower branch, the steady-state solutions are $\langle \hat{a}\rangle_{SS} = \langle \hat{b}\rangle_{SS} = 0$. By taking the noise correlations at steady state, the atomic fluctuations will have no contributions. The second argument is that the number of atoms is very large as in the usual experimental situations, so that the correlations of atomic fluctuations approach zero as N goes to infinity.

We can calculate spectra by using Eqs. (14) and (15). But to see more physical meanings of this composite system, we can rewrite Eqs. (14) and (15) by defining two sets of quadratures

$$\hat{X}_+ = \hat{a} + \hat{a}^\dagger, \quad \hat{X}_- = \frac{\hat{a} - \hat{a}^\dagger}{i}$$ (16)

and

$$\hat{Z}_+ = \hat{b} + \hat{b}^\dagger, \quad \hat{Z}_- = \frac{\hat{b} - \hat{b}^\dagger}{i} .$$ (17)

From these standard definitions, one realizes that $\hat{X}_+$ and $\hat{X}_-$ are just the unsqueezed and squeezed quadratures with relative phase angle $\theta = 0$ for the DOPO system. $\hat{Z}_+$ and $\hat{Z}_-$ are the corresponding atomic variables in and out of phase with the unsqueezed field quadrature. To simplify our calculations, we assume that the pumping field ϵ_2 is real.

With the new operators, Eqs. (14) and (15) read

$$\frac{d\hat{X}_+}{dt} = -\lambda_- \hat{X}_+ + \sqrt{N}g\hat{Z}_+ + \hat{\Gamma}_{X_+} ,$$

$$\frac{d\hat{X}_-}{dt} = -\lambda_+ \hat{X}_- + \sqrt{N}g\hat{Z}_- + \hat{\Gamma}_{X_-} ,$$

$$\frac{d\hat{Z}_+}{dt} = -\gamma_\perp \hat{Z}_+ - \sqrt{N}g\hat{X}_+ + \Delta_a \hat{Z}_- ,$$ (18)

$$\frac{d\hat{Z}_-}{dt} = -\gamma_\perp \hat{Z}_- - \sqrt{N}g\hat{X}_- - \Delta_a \hat{Z}_+ ,$$

with

$$\langle \hat{\Gamma}_{X_+}(t)\hat{\Gamma}_{X_+}(t')\rangle = \frac{2\kappa}{\gamma_2}\epsilon_2\delta(t-t') ,$$

$$\langle \hat{\Gamma}_{X_-}(t)\hat{\Gamma}_{X_-}(t')\rangle = -\frac{2\kappa}{\gamma_2}\epsilon_2\delta(t-t') ,$$ (19)

$$\langle \hat{\Gamma}_{X_+}(t)\hat{\Gamma}_{X_-}(t')\rangle = \langle \hat{\Gamma}_{X_-}(t)\hat{\Gamma}_{X_+}(t')\rangle = 0 .$$

The modified effective field "decay" rates (as can be seen later, λ_- can be negative as the pumping field increases) will take the forms

$$\lambda_- \equiv \gamma_1 - \frac{\kappa}{\gamma_2}\epsilon_2 \ ,$$

$$\lambda_+ \equiv \gamma_1 + \frac{\kappa}{\gamma_2}\epsilon_2 \ . \tag{20}$$

By examining Eqs. (18), we see that the four equations will decouple into two independent sets of equations when the atomic frequency detuning $\Delta_a = 0$. Since the atoms and the field have maximum coupling strength in this on-resonance situation, here we will only consider this most significant case.

Setting $\Delta_a = 0$ in Eqs. (18), we have

$$\frac{d}{dt}\begin{bmatrix} \hat{X}_+ \\ \hat{Z}_+ \end{bmatrix} = \begin{bmatrix} -\lambda_- & \sqrt{N}g \\ -\sqrt{N}g & -\gamma_\perp \end{bmatrix}\begin{bmatrix} \hat{X}_+ \\ \hat{Z}_+ \end{bmatrix}$$

$$+ \begin{bmatrix} \frac{2\kappa}{\gamma_2}\epsilon_2 & 0 \\ 0 & 0 \end{bmatrix}^{1/2}\begin{bmatrix} \hat{\eta}_1(t) \\ \hat{\eta}_2(t) \end{bmatrix} \tag{21}$$

and

$$\frac{d}{dt}\begin{bmatrix} \hat{X}_- \\ \hat{Z}_- \end{bmatrix} = \begin{bmatrix} -\lambda_+ & \sqrt{N}g \\ -\sqrt{N}g & -\gamma_\perp \end{bmatrix}\begin{bmatrix} \hat{X}_- \\ \hat{Z}_- \end{bmatrix}$$

$$+ \begin{bmatrix} -\frac{2\kappa}{\gamma_2}\epsilon_2 & 0 \\ 0 & 0 \end{bmatrix}^{1/2}\begin{bmatrix} \hat{\eta}_3(t) \\ \hat{\eta}_4(t) \end{bmatrix} \ , \tag{22}$$

where $\langle \hat{\eta}_i(t) \rangle = 0$ and $\langle \hat{\eta}_i(t)\hat{\eta}_j(t') \rangle = \delta_{ij}\delta(t - t')$. We can write Eqs. (21) and (22) in the standard form

$$\frac{d}{dt}\hat{\mathbf{u}} = \underline{A}\hat{\mathbf{u}} + \underline{D}^{1/2}\hat{\eta}(t) \ , \tag{23}$$

with

$$\hat{\mathbf{u}}_+ \equiv \begin{bmatrix} \hat{X}_+ \\ \hat{Z}_+ \end{bmatrix}, \quad \underline{A}_+ \equiv \begin{bmatrix} -\lambda_- & \sqrt{N}g \\ -\sqrt{N}g & -\gamma_\perp \end{bmatrix} \ ,$$

$$\underline{D}_+ \equiv \begin{bmatrix} \frac{2\kappa}{\gamma_2}\epsilon_2 & 0 \\ 0 & 0 \end{bmatrix} \ , \tag{24}$$

and

$$\hat{\mathbf{u}}_- \equiv \begin{bmatrix} \hat{X}_- \\ \hat{Z}_- \end{bmatrix}, \quad \underline{A}_- \equiv \begin{bmatrix} -\lambda_+ & \sqrt{N}g \\ -\sqrt{N}g & -\gamma_\perp \end{bmatrix} \ ,$$

$$\underline{D}_- \equiv \begin{bmatrix} -\frac{2\kappa}{\gamma_2}\epsilon_2 & 0 \\ 0 & 0 \end{bmatrix} \ . \tag{25}$$

Notice that the nonzero diffusion element in $\underline{D}_-$ is negative due to the squeezing of the DOPO.

Before starting to study the fluctuation properties of this system, we should take a close look at the deterministic behaviors of this system, particularly the eigenvalues of Eqs. (21) and (22). The deterministic eigenvalues are

$$\lambda_{1,2} = -\tfrac{1}{2}\gamma_\perp\{\mu(1-y)+1$$

$$\pm([\mu(1-y)-1]^2 - 8\mu C)^{1/2}\} \ , \tag{26}$$

which corresponds to (21),

$$\lambda_{3,4} = -\tfrac{1}{2}\gamma_\perp\{\mu(1+y)+1$$

$$\pm([\mu(1+y)-1]^2 - 8\mu C)^{1/2}\} \ , \tag{27}$$

which corresponds to (22).

It can be proved that when

$$\mu C \le \tfrac{1}{2} \ , \tag{28}$$

the lower branch is always stable up to the lower turning point of the bistable curve $y = 1 + 2C$. Otherwise, the lower branch is stable only below $y_{\text{in}} = (1+\mu)/\mu$. Many interesting dynamic properties might appear in the unstable region:

$$\frac{1+\mu}{\mu} < y < 1 + 2C \ . \tag{29}$$

Here, we are going to concentrate only on the stable regions. Even in the stable regions, special features in the atomic and field transmission spectra will appear in different physical allowable regions of parameters μ, C, and y. When

$$[\mu(1-y)-1]^2 - 8\mu C < 0 \tag{30}$$

or

$$[\mu(1+y)-1]^2 - 8\mu C < 0 \ , \tag{31}$$

for given parameters, the eigenvalues of (26) or (27) become complex values, which give two symmetric spectral peaks shifted from the center frequency with the same linewidth for each quadrature field ("double peaks"). In this case we consider the system to be in the strong-coupling limit. When conditions (30) and (31) are not satisfied, the spectra will become two peaks both centered at the center frequency but with a different linewidth for each quadrature field ("single peak"). For a given C value, the spectra can appear as "single peak" for both small μ ("good-cavity" limit) and large μ ("bad-cavity" limit).

IV. OPTICAL AND ATOMIC SPECTRA

We can calculate spectra for those two sets of Eqs. (23)–(25) separately by

$$\underline{S}_\pm(\omega) = (i\omega\underline{I} + \underline{A}_\pm)^{-1}\underline{D}_\pm(-i\omega\underline{I} + \underline{A}_\pm^T)^{-1} \ , \tag{32}$$

where

$$\underline{S}_\pm(\omega) \equiv \begin{bmatrix} (S_{11})_\pm & (S_{12})_\pm \\ (S_{21})_\pm & (S_{22})_\pm \end{bmatrix}$$

$$\equiv \begin{bmatrix} \langle \hat{X}_\pm\hat{X}_\pm \rangle(\omega) & \langle \hat{X}_\pm\hat{Z}_\pm \rangle(\omega) \\ \langle \hat{Z}_\pm\hat{X}_\pm \rangle(\omega) & \langle \hat{Z}_\pm\hat{Z}_\pm \rangle(\omega) \end{bmatrix} \ , \tag{33}$$

and $\underline{I}$ is the unit matrix. Obviously, for these steady-state spectra, the nature of the eigenvalues has a strong effect on the structures of the spectra. Real or complex eigen-

values divide the decomposition of the field transmission spectra into two distinguishable forms. For Eqs. (30) and (31) to be satisfied, i.e., $\lambda_{1,2}$ and $\lambda_{3,4}$ to be complex, the fluctuation spectra for the two field quadratures have the following forms:

$$(S_{11})_{+}^{\text{out}} = 2\gamma_1 \langle \hat{X}_+ \hat{X}_+ \rangle (\Omega)$$

$$= \frac{2\mu^2 y}{\Omega_{0-}^2 + \frac{1}{4}\Gamma_-^2} \left\{ \frac{1 + \frac{\Omega}{2\Omega_{0-}}(1 - \Omega_{0-}^2 - \frac{1}{4}\Gamma_-^2)}{(\Omega + \Omega_{0-})^2 + \frac{1}{4}\Gamma_-^2} \right.$$

$$\left. + \frac{1 - \frac{\Omega}{2\Omega_{0-}}(1 - \Omega_{0-}^2 - \frac{1}{4}\Gamma_-^2)}{(\Omega - \Omega_{0-})^2 + \frac{1}{4}\Gamma_-^2} \right\} \tag{34}$$

and

$$(S_{11})_{-}^{\text{out}} = 2\gamma_1 \langle \hat{X}_- \hat{X}_- \rangle (\Omega)$$

$$= \frac{-2\mu^2 y}{\Omega_{0+}^2 + \frac{1}{4}\Gamma_+^2} \left\{ \frac{1 + \frac{\Omega}{2\Omega_{0+}}(1 - \Omega_{0+}^2 - \frac{1}{4}\Gamma_+^2)}{(\Omega + \Omega_{0+})^2 + \frac{1}{4}\Gamma_+^2} \right.$$

$$\left. + \frac{1 - \frac{\Omega}{2\Omega_{0+}}(1 - \Omega_{0+}^2 - \frac{1}{4}\Gamma_+^2)}{(\Omega - \Omega_{0+})^2 + \frac{1}{4}\Gamma_+^2} \right\} , \tag{35}$$

where

$$\Omega_{0-} \equiv \{2\mu C - \frac{1}{4}[\mu(1-y)-1]^2\}^{1/2} ,$$

$$\Gamma_- \equiv \mu(1-y) + 1 ,$$

$$\Omega_{0+} \equiv \{2\mu C - \frac{1}{4}[\mu(1+y)-1]^2\}^{1/2} , \tag{36}$$

$$\Gamma_+ \equiv \mu(1+y) + 1 ,$$

with $\Omega = \omega/\gamma_\perp$ as the normalized frequency.

$(S_{11})_-^{\text{out}}$ is the fluctuation spectrum for the squeezed quadrature of the DOPO with negative weight and $(S_{11})_+^{\text{out}}$ corresponds to the noisy quadrature. Each of these quadratures has two spectral components centered at $\pm\Omega_{0-}$ or $\pm\Omega_{0+}$, respectively. Notice that these spectral shapes are not standard Lorentzian. These double peaks in the spectral shape are due to the strong interaction between cavity field and two-level atoms. The difference between this splitting and the conventional "vacuum Rabi splitting" is the dependence of the driving field on the splitting frequency.

If the eigenvalues $\lambda_{1,2}$ and $\lambda_{3,4}$ are all real, the spectrum for each quadrature field still has two spectral components, but both are centered at zero frequency and have different linewidths, as

$$(S_{11})_+^{\text{out}} = 2\gamma_1 \langle \hat{X}_+ \hat{X}_+ \rangle (\Omega)$$

$$= \frac{4\mu^2 y}{\Gamma_2^2 - \Gamma_1^2} \left[\frac{\Gamma_2^2 - 1}{\Omega^2 + \Gamma_2^2} - \frac{\Gamma_1^2 - 1}{\Omega^2 + \Gamma_1^2} \right] \tag{37}$$

and

$$(S_{11})_-^{\text{out}} = 2\gamma_1 \langle \hat{X}_- \hat{X}_- \rangle (\Omega)$$

$$= -\frac{4\mu^2 y}{\Gamma_4^2 - \Gamma_3^2} \left[\frac{\Gamma_4^2 - 1}{\Omega^2 + \Gamma_4^2} - \frac{\Gamma_3^2 - 1}{\Omega^2 + \Gamma_3^2} \right] , \tag{38}$$

where

$$\Gamma_1 = \frac{1}{2}[1 + \mu(1-y) + \{[\mu(1-y)-1]^2 - 8\mu C\}^{1/2}] ,$$

$$\Gamma_2 = \frac{1}{2}[1 + \mu(1-y) - \{[\mu(1-y)-1]^2 - 8\mu C\}^{1/2}] ,$$

$$\Gamma_3 = \frac{1}{2}[1 + \mu(1+y) + \{[\mu(1+y)-1]^2 - 8\mu C\}^{1/2}] ,$$

$$\Gamma_4 = \frac{1}{2}[1 + \mu(1+y) - \{[\mu(1+y)-1]^2 - 8\mu C\}^{1/2}] .$$

$$\tag{39}$$

Typical spectral shapes for both quadratures are given in Figs. 2–5. At different parameter regions, the fluctuation spectra for both quadrature components may have different structures as discussed above.

For the given parameters of $\mu = 100$ ("bad cavity") and $C = 1$, λ_1 in Eq. (26) will change from real to complex at $y = 0.71$. Figure 2 plots the quadrature $\langle \hat{X}_+ \hat{X}_+ \rangle (\Omega)$ as a function of Ω with increasing pumping strength y. Below $y = 0.71$, the spectrum is determined by Eq. (37) with two Lorentzian line shapes centered at zero frequency and different linewidths Γ_1 and Γ_2 given in (39), as shown in Fig. 3(a). The dashed and dotted curves are the two Lorentzian components of Eq. (37) and the solid curve is the sum of these two components. The negative narrow spectral component creates a hole in the positive broad spectrum. Since the pumping field $y = 0.25$ is far from the unstable point of $y_{\text{in}} = 1.01$ in this case ($\mu C > \frac{1}{2}$), the amplitude of the spectrum is relatively small. When the pumping field y is increased and crosses the point of $y = 0.71$, the spectrum will be governed by Eq. (34) with two spectral components centered at $\pm\Omega_{0-}$. Since Eq. (34) has two non-Lorentzian line shapes, some rather interesting spectral shapes can appear for each spectral component, as shown in Fig. 3(b). The dashed and dotted lines are for each component in (34), respectively. Each component has an unsymmetric line shape and has negative values in some regions, but the sum of these two will
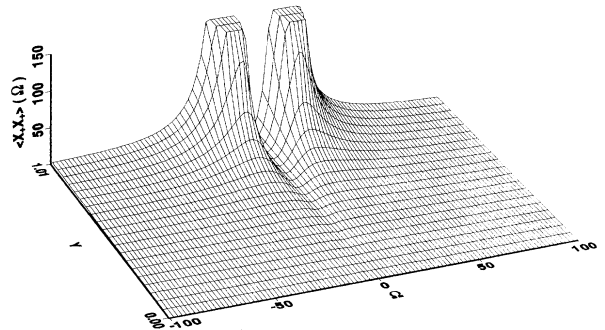
FIG. 2. Fluctuation spectrum $\langle X_+ X_+ \rangle (\Omega)$ vs Ω and pumping intensity Y in the bad-cavity limit. The parameters are $\mu = 100$ and $C = 1.0$. The instability point in this case is at $y_{\text{in}} = 1 + 1/\mu = 1.01$.

OPTICAL SPECTRA FROM A DEGENERATE OPTICAL...

give a spectral shape similar to Fig. 3(a) with all values above zero. With further increase of pumping strength to $y = 1.0$, the gap between the two peaks on the spectrum will become larger and larger, and the spectrum will then simply look like two peaks centered at $\pm\Omega_{0-}$ with the same linewidth. The spectrum is determined by Eq. (34) and plotted in Fig. 3(c). Since condition (11) is satisfied
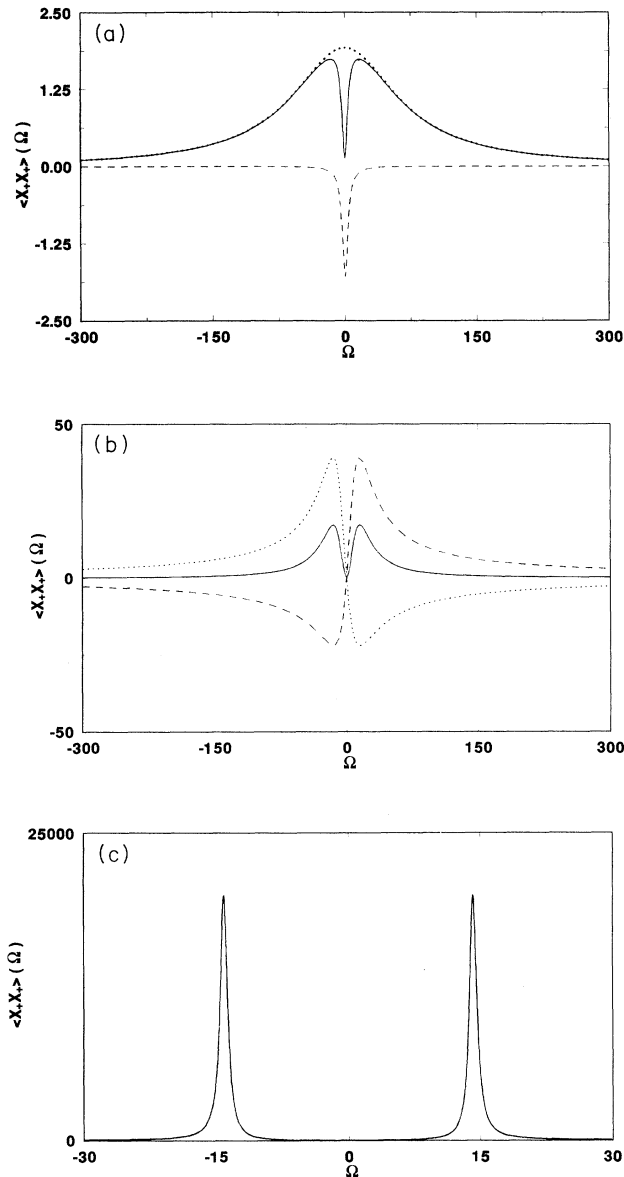
FIG. 3. Different structures of spectra for X_+ quadrature in the bad-cavity limit, with $\mu = 100$ and $C = 1.0$. The critical point for the eigenvalue is $y_c = 0.71$. (a) $y = 0.25$ ($y < y_c$). Dotted and dashed curves are two spectral components in Eq. (37). The solid curve is the total spectrum $\langle X_+ X_+ \rangle(\Omega)$. (b) $y = 0.72$ ($y \approx y_c$). Dotted and dashed curves are two spectral components in Eq. (34). The solid curve is the total spectrum $\langle X_+ X_+ \rangle(\Omega)$. (c) $y = 1.0$ ($y > y_c$). Spectrum $\langle X_+ X_+ \rangle(\Omega)$ is given by Eq. (34) with two separate spectral peaks.

for the given parameters, this system becomes unstable at $y_{in} = (1+\mu)/\mu = 1.01$, which is below the lower turning point of the bistable curve of $y_{in} = 1 + 2C = 3.0$. From Fig. 2 one can see that, as the pumping amplitude approaches the instability point, the amount of fluctuations increases dramatically until the point where the weak-field assumption breaks down. Although Fig. 2 shows a smooth spectrum as y increases, the spectrum actually has different intrinsic structures. It is clear that when the pumping amplitude increases from zero, the amount of squeezing increases. Since the eigenvalues $\lambda_{3,4}$ in (27) are always real for the given parameters, the spectrum is governed by Eq. (38). The spectrum is basically given by a broad negative spectrum due to DOPO and by a narrow positive peak due to atomic resonance absorption (since $\mu \gg 1$, the atomic linewidth is much narrower than the cavity linewidth), as shown in Fig. 4(b), which is a slide plot of Fig. 4(a) with $y = 1.0$. As demonstrated in Fig. 4(a), when y approaches the unstable point of $y_{in} = (1+\mu)/\mu = 1.01$, the best output squeezing can approach the perfect value of -1 at a frequency outside the atomic resonance peak.

The field spectra will be different in the good-cavity limit. Since condition (28) is satisfied for the given parameters, the system is stable up to $y_{in} = 1 + 2C = 3.0$.
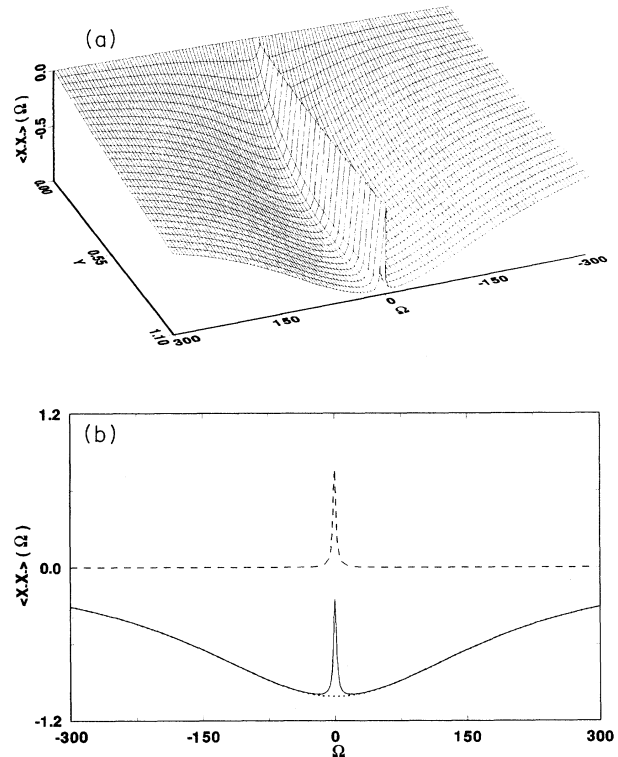
FIG. 4. (a) Fluctuation (squeezing) spectrum $\langle X_- X_- \rangle(\Omega)$ vs Ω and pumping intensity Y in the bad-cavity limit. All the parameters are the same as in Fig. 2. The instability point in this case is $y_{in} = 1.01$. (b) A cross-section cut of Fig. 4(a) for $y = 1.0$. The dotted and dashed curves are the two spectral components of Eq. (38) and the solid curve is the total spectrum.
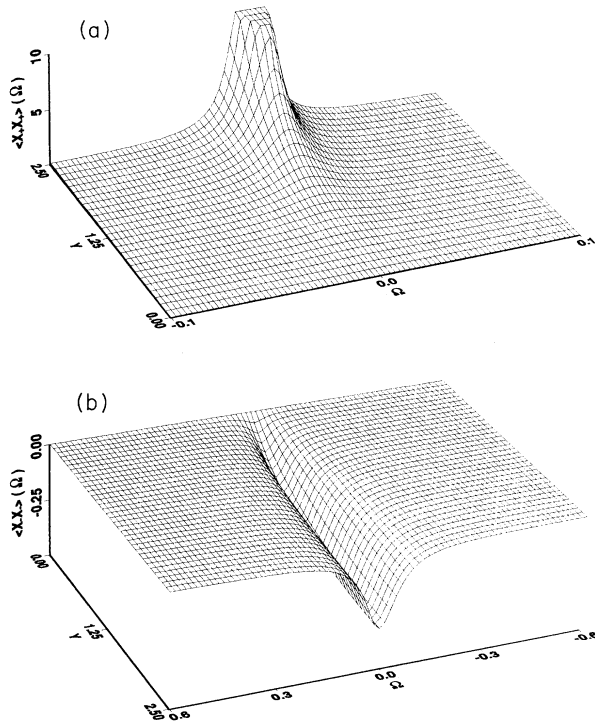
FIG. 5. Fluctuation spectra vs Ω and pumping intensity Y in the good-cavity limit, with $\mu=0.01$ and $C=1.0$ for (a) $\langle X_+X_+ \rangle(\Omega)$, and (b) $\langle X_-X_- \rangle(\Omega)$.

For these given parameters, the eigenvalues are always real. The spectra are governed by Eq. (37), which has two Lorentzian peaks at center frequency. The linewidth of this spectrum is determined by the linewidths of the two Lorentzian components Γ_1 and Γ_2 in Eq. (39). Figure 5(a) plots the quadrature $\langle \hat{X}_+\hat{X}_+ \rangle(\Omega)$ as a function of Ω with increasing pumping strength y for the "good-cavity" limit of $\mu=0.01$ and the same $C=1.0$. Since the two spectral components in (37) are all positive for this case, there will be no hole in the center of the spectra. As the pumping amplitude y increases to the threshold value, the fluctuation spectrum increases until the weak-field assumption breaks down. Figure 5(b) plots $\langle \hat{X}_-\hat{X}_- \rangle(\Omega)$ as a function of Ω with increasing pumping strength y for the same parameters as in Fig. 5(a). These spectra are given by Eq. (38) and exhibit simple spectral shape with no absorption peak at the center frequency. The amount of squeezing is much smaller than the ideal DOPO output. To achieve perfect squeezing at the output, the single-sided output has to dominate the total losses (including cavity loss, scattering from crystals, and atomic fluorescence) of the system [7]. In this good-cavity limit, the atomic decay rate $\gamma_\perp$ is much larger than the cavity output rate γ_1 ($\mu\equiv\gamma_1/\gamma_\perp \ll 1$). The quantum correlation has been interrupted by the random atomic fluorescence.

When the driving field y is close to the modified threshold value $1+2C$ or the instability point $(1+\mu)/\mu$, depending on the parameters, the power of the positive quadrature $\langle \hat{X}_+\hat{X}_+ \rangle(\Omega)$ will be much larger than that of the negative quadrature $\langle \hat{X}_-\hat{X}_- \rangle(\Omega)$, so the total incoherent spectrum is dominated by the positive quadrature. Since there is no coherent field at this subharmonic frequency inside the cavity, these incoherent transmission spectra will be much easier to detect experimentally. If both conditions (30) and (31) are satisfied, there will be four peaks in the transmission spectra. These peaks are due to both the DOPO (λ_+ and λ_-) and the strong coupling between the intracavity field and atoms ($Ng^2 \geq \gamma_1^2$). Although the squeezed quadrature is relatively small in amplitude, we can still detect it by a heterodyne detection technique.

Similarly, the conditions of (30) and (31) also divide the atomic transmission spectra into two different forms. The positive quadrature $\langle \hat{Z}_+\hat{Z}_+ \rangle(\Omega)$ of the collective atomic fluctuation spectrum is always associated with the noisy field quadrature $\langle \hat{X}_+\hat{X}_+ \rangle(\Omega)$ and the negative quadrature $\langle \hat{Z}_-\hat{Z}_- \rangle(\Omega)$ with the squeezed field quadrature $\langle \hat{X}_-\hat{X}_- \rangle(\Omega)$. These are collective atomic spectra. The atomic fluorescence spectra have to be calculated with a different method.

Actually, simple relations exist between output field spectra and output atomic spectra since they are two diagonal components in the matrix (33). By solving the matrix Eq. (32), we have

$$\langle \hat{Z}_+\hat{Z}_+ \rangle(\Omega) = \frac{2\mu C}{1+\Omega^2}\langle \hat{X}_+\hat{X}_+ \rangle(\Omega) \tag{40}$$

and

$$\langle \hat{Z}_-\hat{Z}_- \rangle(\Omega) = \frac{2\mu C}{1+\Omega^2}\langle \hat{X}_-\hat{X}_- \rangle(\Omega) . \tag{41}$$

The total output atomic spectrum is defined as the sum of both quadratures

$$
\begin{aligned}
S_A^{\text{out}}(\Omega) &= 2\gamma_\perp[\langle \hat{Z}_+\hat{Z}_+ \rangle(\Omega)+\langle \hat{Z}_-\hat{Z}_- \rangle(\Omega)] \\
&= \frac{2C}{1+\Omega^2}\{2\gamma_1[\langle \hat{X}_+\hat{X}_+ \rangle(\Omega)+\langle \hat{X}_-\hat{X}_- \rangle(\Omega)]\} \\
&= \frac{2C}{1+\Omega^2}[(S_{11})_+^{\text{out}}+(S_{11})_-^{\text{out}}] ,
\end{aligned} \tag{42}
$$

where $(S_{11})_+^{\text{out}}$ and $(S_{11})_-^{\text{out}}$ are given in Eqs. (34) and (35) or (37) and (38) depending on the conditions (30) and (31).

The interesting feature is that the negative atomic quadrature, which couples to the "squeezed field quadrature," has a linewidth larger than the atomic natural linewidth. On the contrary, the positive quadrature, which couples to the "unsqueezed field quadrature," can have a subnatural atomic linewidth. The total atomic spectrum is the sum of the spectra from the two quadratures. As the pumping field increases towards the modified threshold or the unstable point, the linewidth of the atomic spectrum becomes narrower and narrower, as for a laser near its threshold. The half-width at half maximum of the atomic spectrum can be estimated by only considering the dominated positive quadrature, which gives

$$\Delta\Omega = \tfrac{1}{2}\Gamma_- \left\{ -\frac{\Gamma_-}{2\Omega_{0-}} + \left[\left[\frac{\Gamma_-}{2\Omega_{0-}} \right]^2 + 1 \right]^{1/2} \right\} , \tag{43}$$

where Γ_- and Ω_{0-} are given in (36). When $\Gamma_-=0$, i.e., $y=(1+\mu)/\mu$, the linewidth $\Delta\Omega$ will be zero (at this point the weak-field approximation will break down). At the same time, the negative quadrature always has linewidths larger than the natural linewidth.

This phenomenon can be understood, in a language used by Carmichael et al. in another system [11], as the following: the total decay rate of this composite system is split into $\frac{1}{2}(\lambda_\pm+\gamma_\perp)$, where the modified cavity decay rates $\lambda_\pm$ replace the cavity decay rate in Ref. [11]. In their system (AOB), Carmichael et al. argued that if the cavity decay rate were very small compared to the atomic decay rate, then the decay rate of the system would be $\frac{1}{2}\gamma_\perp$. In our system,

$$\lambda_-\equiv\gamma_1-\frac{\kappa\epsilon_2}{\gamma_2}\equiv\gamma_1(1-y) \qquad (44)$$

can be negative for

$$1<y<\frac{1+\mu}{\mu}=\frac{\gamma_1+\gamma_\perp}{\gamma_1}, \qquad (45)$$

which allows $\frac{1}{2}(\lambda_-+\gamma_\perp)$ to be arbitrarily small. This subnatural linewidth has nothing to do with quantum fluctuations and is determined by the dynamics of the system.

When conditions (30) and (31) are not satisfied, the atomic spectra take the forms of Eqs. (37) and (38). Each of the quadratures consists of two Lorentzian components centered at zero frequency with different linewidths.

Figure 6 plots total transmitted atomic spectra in a special case of the bad-cavity limit ($\mu=100$, $C=1$). Since the condition (30) is satisfied, the spectrum splits into two distinguishable peaks centered at $\pm\Omega_{0-}$, as in the inset of Fig. 6(b). The double peaks are due to the strong interaction between the cavity field and atoms. The single peak in this figure is an enlarged version of the right peak in the inset. Since $y=1.009$ is very close to the unstable point of $y_{in}=1.01$ for given parameters μ and C, the linewidth narrowing is mainly caused by the dynamic instability of this system. It is obvious that the peak is much narrower than the atomic natural linewidth, which has a full width at half maximum of unity normalized by $\gamma_\perp$. The contribution from $\langle\hat{Z}_-\hat{Z}_-\rangle(\Omega)$ is very small compared to $\langle\hat{Z}_+\hat{Z}_+\rangle(\Omega)$ in this case. This is in the bad-cavity limit of $\mu\gg1$. For comparison, a spectrum with lower driving intensity ($y=0.5$) is given in Fig. 6(a). In this case, the spectrum has a hole at the zero frequency.

Total transmitted atomic spectrum in the good-cavity limit ($\mu=0.01$ and $C=1.0$, and $y=2.7$) is given in Fig. 7. Since the condition (30) is not satisfied, the eigenvalues $\lambda_{1,2}$ are real, which gives single-peaked spectra. The lower turning point is $y_{th}=3.0$; the fluctuation spectrum increases dramatically, as the pumping intensity increases, until the weak-field assumption breaks down. Of course, the positive quadrature $\langle\hat{Z}_+\hat{Z}_+\rangle(\Omega)$ dominates the total transmitted atomic spectrum near the lower turning point. One can see that the linewidth of this
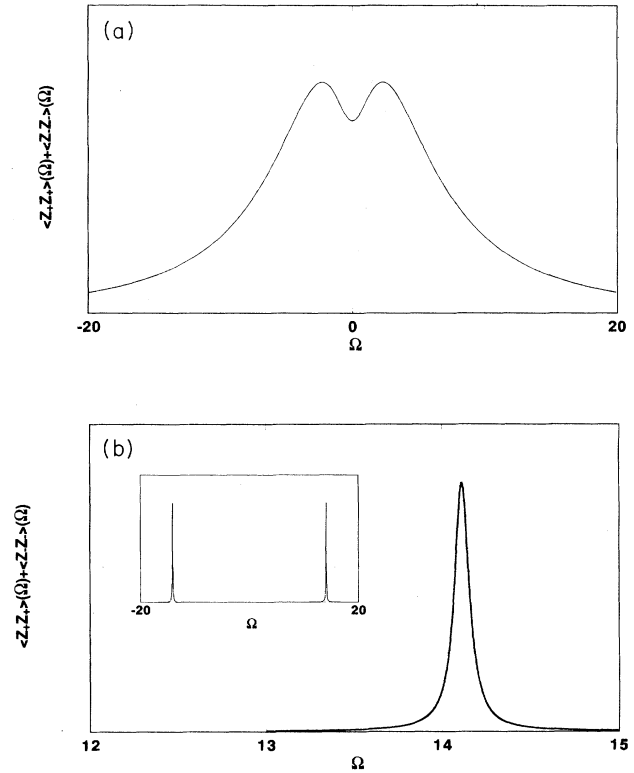
FIG. 6. Total atomic fluctuation spectrum $\langle Z_+Z_+\rangle(\Omega)+\langle Z_-Z_-\rangle(\Omega)$ vs Ω in the bad-cavity limit for $\mu=100$, $C=1.0$, and (a) $y=0.5$, (b) $y=1.009$. The instability point in this case is $y_{in}=1.01$. The vertical axis is in arbitrary units.

spectrum is much narrower than the atomic natural linewidth. This linewidth narrowing in the transmitted atomic spectrum is due to the dynamic behavior of the system near its threshold value.

Although small, the negative sign in the quadrature $\langle\hat{Z}_-\hat{Z}_-\rangle(\Omega)$ [proportional to $\langle\hat{X}_-\hat{X}_-\rangle(\Omega)$ given in (41)] defines the "atomic squeezing," which will not be discussed here.
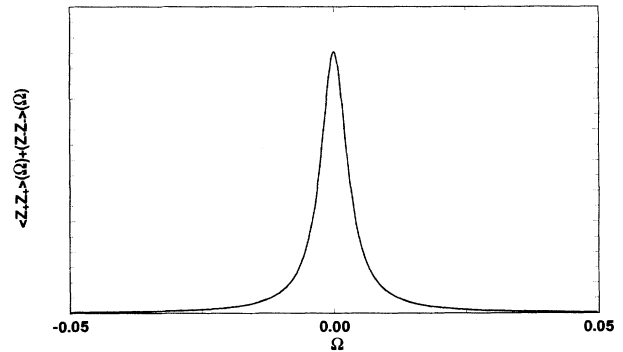
FIG. 7. Total atomic fluctuation spectrum $\langle Z_+Z_+\rangle(\Omega)+\langle Z_-Z_-\rangle(\Omega)$ vs Ω in the good-cavity limit for $\mu=0.01$, $C=1.0$, and $y=2.7$. The system is stable up to $y_{th}=1+2C=3.0$. The vertical axis is in arbitrary units.

V. DISCUSSION

We have studied a composite system of a degenerate optical parametric oscillator coupling with N two-level atoms. This system exhibits bistability in its steady-state intracavity intensity versus pumping intensity. On the lower branch of the steady-state bistable curve, the averaged coherent intensity is always zero. Using this fact, we introduced approximated Schwinger representation in the weak-field limit for the atomic variables and wrote down a set of coupling linear equations for the intracavity field and atomic polarization variables. By transforming atomic and field variables, simultaneously, into appropriate quadratures, we were able to separate these coupled equations, under a resonance condition, into two independent groups. One set of equations involves only the "squeezed field quadrature" and its corresponding atomic quadrature. Another set of equations involves the "unsqueezed field quadrature" and a different atomic quadrature. Atomic detuning couples these two sets of equations.

This transformation allows us to see how the "squeezed" and "unsqueezed" quadratures interact with atoms separately and how they contribute to the atomic spectra or how the atoms change the squeezed spectra from a DOPO. Of course, this study is not complete without the calculation of the atomic fluorescence spectra. Since a very different method will be involved in calculating atomic fluorescence spectra, we will present that study in a separate publication. The collective atomic spectra have different spectral shapes from the intracavity field fluctuation spectra, as given in (40) and (41). When the pumping field approaches the turning point (modified DOPO threshold) or the instability point under Eq. (11), the unsqueezed field spectrum becomes much narrower and its amplitude becomes very large, as for the case of a laser. As the photon number gets too large due to the fluctuations, our weak-field assumption will break down. The negative spectral components (due to squeezing) do contribute to the line narrowing of the atomic spectra, but not as a dominant effect. The main effect of the narrow atomic spectral shape near the unstable points is the dynamic coupling between atoms and the intracavity fundamental field. Equations (26) and (27) define "vacuum Rabi splitting" when they become complex as the "double-peak" cases since the mean intracavity field is zero. As y increases, the eigenvalue changes from real to complex, giving rise to Rabi frequencies Ω_{0+} and Ω_{0-}. Although the steady-state intracavity intensity is still zero for y below the threshold value, the fluctuation field energy due to parametric amplification of frequency down-conversion will be significant. Since each field quadrature has two spectral components, different spectral shapes, under different parameters, can combine to give similar total spectral shapes, as in Figs. 3(a), 3(b), and 3(c). The transmitted squeezing field quadrature can be detected using the heterodyne technique. The parametric gain is very important in obtaining the narrow linewidth because it causes the instability and balances the cavity decay.

As for the total transmitted atomic spectra, we took the pumping parameter near the unstable points in Figs. 6 and 7, therefore the spectra are dominated by the positive atomic quadrature, which couples with the unsqueezed field quadrature. Since there is no coherent spectral component, this system is different compared to the normal atomic optical bistability system studied previously.

When we performed transformation to the quadratures in Eqs. (16) and (17), we took the zero phase $\theta = 0$, as in the DOPO case. From Eqs. (34) and (37) or Figs. 3(a) and 3(b), we see that the "unsqueezed quadrature" actually can have negative components. This is because of the fact that a system of two-level atoms inside an optical cavity without DOPO will produce squeezing at nonzero phase angles [13]. When this system combines with the DOPO, the best squeezing might occur at a new phase angle other than zero.

ACKNOWLEDGMENTS

[1] C. W. Gardiner, Phys. Rev. Lett. **56**, 1917 (1986).

[2] H. J. Carmichael, A. S. Lane, and D. F. Walls, Phys. Rev. Lett. **58**, 2539 (1987).

[3] H. J. Carmichael et al., Phys. Rev. A **40**, 5516 (1989).

[4] P. R. Rice and H. J. Carmichael, J. Opt. Soc. Am. B **5**, 1661 (1988).

[5] M. G. Raizen et al., Phys. Rev. Lett. **63**, 240 (1989).

[6] Min Xiao and S. Z. Jin, Phys. Rev. A **45**, 483 (1992).

[7] L. A. Wu, H. J. Kimble, J. L. Hall, and H. Wu, Phys. Rev. Lett. **57**, 2520 (1987); L. A. Wu, Min Xiao, and H. J. Kimble, J. Opt. Soc. Am. B **4**, 1465 (1987).

[8] G. S. Agarwal and S. D. Gupta, Phys. Rev. A **39**, 2961 (1989).

[9] H. J. Carmichael, Phys. Rev. A **33**, 3262 (1986).

[10] H. W. Louisell, Quantum Statistical Properties of Radiation (Wiley, New York, 1973).

[11] L. A. Orozco, H. J. Kimble, and A. T. Rosenberger, Opt. Commun. **62**, 54 (1987).

[12] M. Lax, Rev. Mod. Phys. **32**, 25 (1960).

[13] M. G. Raizen, L. A. Orozco, Min Xiao, T. L. Boyd, and H. J. Kimble, Phys. Rev. Lett. **59**, 198 (1987).